RAMAN SPECTROSCOPY AND X-RAY DIFFRACTION CHARACTERIZATION OF AMORPHOUS FERRIC SULFATE-BEARING SALTS: APPLICATION TO MSL, MARS 2020 AND EXOMARS DATA.

J. C. Gregerson[1*], A. D. Rogers[1], M. Zaman[2], E. C. Sklute[3], L. Ehm[1,4], J. B. Parise[1,4], [1]Stony Brook University, Stony Brook, NY 11794-2100, jason.gregerson@stonybrook.edu. [2]Cornell University, Ithaca, NY. [3]Planetary Sci. Inst. Tucson AZ. [4]Brookhaven National Lab, Upton, NY.

Introduction: The Mars Science Laboratory Curiosity rover mission discovered a significant fraction of x-ray amorphous material in Martian soils at Gale crater using the CheMin X-ray diffractometer [1]. Based on the chemical characteristics, the x-ray amorphous fraction is likely a combination of amorphous or nanocrystalline phases, and could include silicate glass, allophane, nanophase iron oxides, amorphous salts, and/or other poorly crystalline silicate weathering products [e.g. 2]. Understanding which phases compose the amorphous fraction is important for understanding the long-term evolution, mechanical properties, and biosignature preservation potential of Martian soils.

A distinctive aspect of the amorphous component chemistry is that it contains nearly the entire bulk soil budget of sulfur and H_2O [3, 4]. Hypothesized candidate phases for the sulfur-bearing component include amorphous sulfates [2, 5] or sulfate-bearing solid solutions [6], and/or chemisorbed SO_4 onto nanophases such as allophane or ferrihydrite [2, 7]. Chemisorbed SO_4 is a common occurrence in terrestrial volcanic soils [7-9], whereas amorphous ferric sulfate or sulfate-bearing solid solutions are expected end products of rapid ferric sulfate or multicomponent brine dehydration [6, 10]. Rapid dehydration would be expected under the low pressure conditions of the Martian atmosphere.

One potential way to distinguish between these viable candidate phases is via Raman and VNIR spectroscopy. The Mars 2020 SuperCam instrument will contain a remote Raman spectrometer with a 532 nm laser and a VNIR reflectance spectrometer [11] and the SHERLOC instrument contains a micro-imaging Raman spectrometer utilizing a 248 nm laser [12]. The ExoMars rover will include a Raman spectrometer utilizing a 532 nm laser [13] and a micro-VNIR micro-imaging spectrometer [14]. VNIR spectra of amorphous ferric sulfate-bearing phases were already presented by Sklute et al. [5, 6] and VNIR spectra of chemisorbed SO_4 complexes were presented by Rampe et al. [7]. In this work, we present Raman spectra of amorphous ferric sulfate and amorphous solid solutions of ferric sulfate – sodium chloride. In our future work we will acquire Raman spectra of allophane and ferrihydrite with chemisorbed SO_4 for comparison to the Raman spectra of amorphous ferric sulfates.

Samples and sample synthesis: Five sulfate-bearing amorphous samples and one crystalline anhydrous ferric sulfate sample were synthesized (**Table 1**). Anhydrous $Fe_2(SO_4)_3$ (99.998% purity) was deliquesced in a 99% RH environment buffered by deionized water to form a solution with a concentration of 32.3wt% $Fe_2(SO_4)_3$. Chloride solutions were made by dissolving solid NaCl and $MgCl_2$ in deionized water to make a 17.6wt% NaCl solution and a 18.5wt% $MgCl_2$ solution.

Table 1. Composition of dehydration products* analyzed by Raman spectroscopy

Brine label	Molar composition			XRD
	Fe^{3+} sulfate	Chloride	H_2O	
$Fe_2(SO_4)_3$	1	0	4.4	amorphous
$Fe_2(SO_4)_3$ + NaCl	1	1.3	3.5	amorphous
$Fe_2(SO_4)_3$ + 2NaCl	1	2.3	1.7	amorphous
$Fe_2(SO_4)_3$ + $MgCl_2$	1	1.2	4.1	amorphous
$Fe_2(SO_4)_3$ + 2$MgCl_2$	1	2.2	6.9	amorphous + crystalline

*Because amorphous solids can form from rapid dehydration of both pure and multicomponent brines [6], sulfate-chloride mixtures were included in our analyses.

The $Fe_2(SO_4)_3$ solution was mixed with each chloride on a molar ratio of 1:1 and 1:2. These four mixtures, along with the pure $Fe_2(SO_4)_3$ solution were dehydrated via vacuum for seven days in an attempt to form amorphous solids as per Sklute et al., 2015 [5]. Samples were weighed before and after dehydration to determine hydration state. The resulting dehydration products form ochre-colored powders.

Sample Analysis Methods: Samples were analyzed in a N_2-purged atmosphere under ambient temperatures. Raman spectra were acquired with a B&W Tek iRamanPlus portable spectrometer using a 532 nm laser, under 50mW power for 30-120 s. X-ray diffraction (XRD) patterns for the same samples were then acquired to verify their amorphous state. The XRD patterns were measured using an Olympus BTX-II with a 30 kV Co anode micro-focus X-ray source. The BTX-II shares a similar transmission configuration and angular range and resolution (5-55° 2θ, 0.25° 2θ FWHM) with CheMin.

Results: The XRD data confirm that all but the 1:2 mixture of $Fe_2(SO_4)_3$ and $MgCl_2$ are fully X-ray amorphous (**Fig. 1**). The outlier sample which shows peaks from an unknown crystalline phase is superposed on a broad diffuse scattering pattern, suggesting it is a mixture of amorphous and crystalline material.

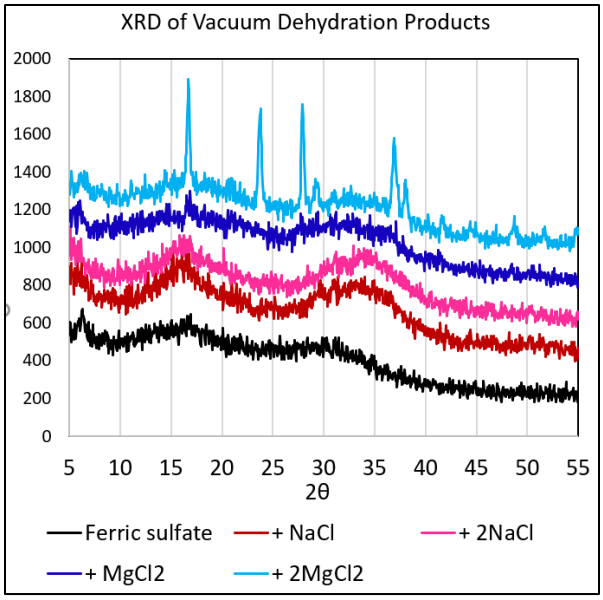

Figure 1. XRD patterns for each of the samples in this work. The patterns in this figure are offset to show detail.

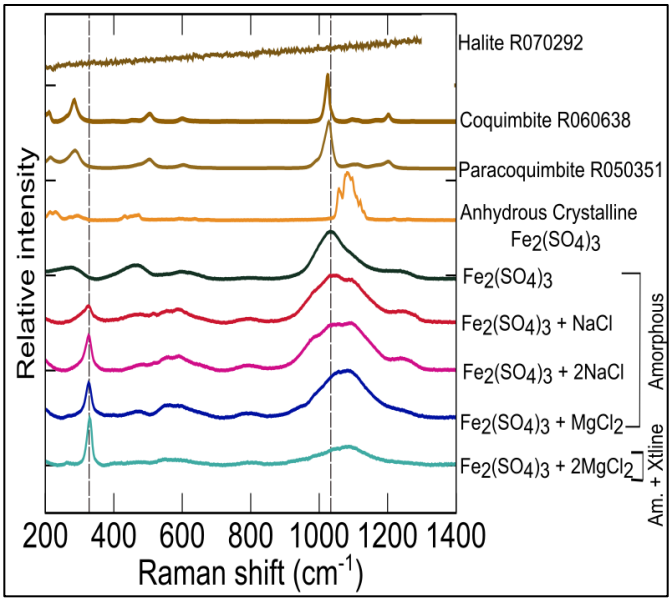

Figure 2. Raman spectra of anhydrous crystalline ferric sulfate and amorphous sulfate-bearing phases. Other crystalline ferric sulfates (coquimbite, paracoquimbite) and halite are shown for comparison. Reference samples are from the RRUFF database. Vertical dashed lines are placed at 330 cm^{-1} and 1034 cm^{-1}.

Raman spectra (**Fig. 2**) show a significant difference between pure amorphous and crystalline ferric sulfate, with both a broadening and shifting of the major SO_4 asymmetric stretching mode from 1086 cm^{-1} to 1034 cm^{-1}. A noticeable difference in the lattice vibrational modes <900 cm^{-1} is also observed. Raman signatures of chloride-containing phases exhibit peak broadening and shifting of the SO_4 asymmetric stretching mode near 1034 cm^{-1} relative to pure amorphous ferric sulfate. A sharp peak near 330 cm^{-1} is also present in the chloride-bearing samples but lacking in the pure ferric sulfate. Though not shown in Figure 2, all of the brine dehydration products show a broad feature at 2414 cm^{-1} due to H_2O.

Discussion: Based on comparison with Raman spectra of ferric sulfates presented by [15], the SO_4 peak shift observed between the anhydrous crystalline sulfate and the pure amorphous ferric sulfate (approximately 5 structural H_2O) is likely due to differences in hydration state. In [15], no peak *shift* between crystalline pentahydrate and amorphous ferric sulfate, which both have approximately the same level of hydration, was observed. However, the peak *broadening* may be attributed to the structural changes associated with amorphization. The sharp peak at 330 cm^{-1} in the chloride-bearing samples suggests the presence of an unidentified crystalline phase. The lack of sharp peaks in the XRD patterns suggest that the phase is likely nano-crystalline.

Future work will include Raman spectroscopy of a range of amorphous ferric sulfates of varying hydration state, and of chemisorbed SO_4 on Fe-bearing and Si/Al-bearing nanophases.

Acknowledgements: This work was supported by the NASA SSW and PME awards 80NSSC18K0535 and 80NSSC18K0516.

References: [1] Bish, D. L., et al. (2013). *Science*, 341(6153), 1238932. https://doi.org/10.1126/science.1238932 [2] McAdam, A. C., et al. (2014). *JGR-Planets, 119*, 1-21. [3] Leshin, et al. (2013). *Science*, 341, 1–10. [4] Dehouck, E., et al. (2014). *JGR-Planets*, *119*(12), 2640–2657 [5] Sklute, E. C., et al. (2015). *JGR-Planets*, 120(4), 809–830. https://doi.org/10.1002/2014JE004784 [6] Sklute, E. C., et al. (2018). *Icarus*, 302, 285–295. https://doi.org/10.1016/j.icarus.2017.11.018 [7] Rampe, E. B., et al. (2016), *Am. Min.*, *101*, 678–689. [8] Parfitt, R. L. and R. S. C. Smart (1978), *Soil Sci. Soc. Am. J.*, *42*(1), 48–50. [9] Ishiguro, M., & Makino, T. (2011). *Colloids and Surfaces A: Physicochemical and Engineering Aspects, 384(1–3)*, 121–125. https://doi.org/10.1016/j.colsurfa.2011.03.040 [10] Xu, W. Q., et al. (2009). *Am. Min.*, *94*(11–12), 1629–1637. https://doi.org/10.2138/am.2009.3182 [11] Wiens, R. C., et al. (2017) *Spectroscopy*, *32*(5), 50–55. [12] Beegle, et al. (2015). *IEEE Aero. Proc.*, *June*, 1–11. https://doi.org/10.1109/AERO.2015.7119105 [13] Rull, F., et al. (2017). *Astrobiology*, *17*(6–7), 627–654. https://doi.org/10.1089/ast.2016.1567 [14] Bibring, J.-P., & the MicrOmega Team (2017). *Astrobiology*, *17*(6–7), 621–626. https://doi.org/10.1089/ast.2016.1642 [15] Ling, Z. C., & Wang, A. (2010) *Icarus*, 209(2), 422–433. https://doi.org/10.1016/j.icarus.2010.05.009